The Astronomical Journal, 135:400–407, 2008 January doi:10.1088/0004-6256/135/1/400
© 2008. The American Astronomical Society. All rights reserved. Printed in the U.S.A.

DEEP SEARCH FOR CARBON MONOXIDE IN COMETARY PRECURSORS USING MILLIMETER WAVE SPECTROSCOPY*

David Jewitt, Catherine A. Garland[1], and Herve Aussel[2]
Institute for Astronomy, University of Hawaii, 2680 Woodlawn Drive, Honolulu, HI 96822, USA; jewitt@ifa.hawaii.edu
Received 2007 August 7; accepted 2007 September 18; published 2007 December 12

ABSTRACT

Carbon monoxide is abundant in comets and is volatile throughout most of the planetary region of the solar system, raising the possibility that it might be detectable in the cometary precursor classes known as the Centaurs and the Kuiper belt objects (KBOs). In this paper we present a search for carbon monoxide in Centaurs and Kuiper belt objects focused on the $J = 2$–1 rotational transition at 230 GHz. No CO emission is detected. We use upper limits from the radio spectra to infer that the surfaces of these objects are strongly depleted in supervolatile ices: CO can cover no more than 0.1–1% of the surface area. Two possibilities for the survival of sub-surface CO ice are considered. First, bulk CO ice could survive undetected at depths much greater than the annual thermal skin depth. Inward drift of the perihelion distance would allow heat conducted from the surface to reach the CO ice, driving outgassing through short-lived vents at rates generally too small to be detected. Second, CO might be physically trapped within a porous, amorphous ice matrix and released where the local temperatures are sufficient to promote the transformation of amorphous into crystalline ice. In either case, the non-detections in our data would reflect the large perihelia and low temperatures of the sampled objects but would not set useful constraints on the interior abundances of CO or other supervolatiles.

Key words: comets: general – Kuiper Belt – radio lines: solar system – solar system: formation

1. INTRODUCTION

The comets are volatile-rich interplanetary bodies which lose mass by sublimation in response to heating by the Sun. Most known comets are sufficiently small that the observed rates of mass loss cannot be sustained for much more than 10^4–10^5 years. These bodies must have recently arrived in the inner solar system from more distant, cold source regions. One likely source is the Kuiper belt, which sends a continuous rain of bodies to be scattered throughout the solar system by strong gravitational interactions with the giant planets (Fernandez 1980; Duncan et al. 1988). Objects which have recently escaped the Kuiper belt and whose dynamics are controlled by the giant planets are known as Centaurs. Centaurs which cross the orbit of Jupiter are heated by the Sun to temperatures high enough to sublimate water ice and are then re-labeled as the Jupiter Family Comets (JFCs). Prolonged exposure to the Sun leads to the depletion of volatiles within a few thermal skin depths of the surfaces, and outgassing activity on the JFCs becomes restricted to a few, small "active areas" on the nucleus. Eventually, mass loss may shut down completely. Such "inactive" or "dormant" comets are likely to be classified by ground-based observers as asteroids, albeit ones with orbits that are distinct from those of asteroids in the main belt between Mars and Jupiter (Hartmann et al. 1987; Jewitt 2005).

Cometary outgassing at heliocentric distances smaller than 5 AU or 6 AU is controlled by the thermodynamics of water ice sublimation (Whipple 1950). At larger distances (perhaps up to 7 AU or 8 AU) and lower temperatures, it has been suggested that transformations of water ice from the amorphous to the crystalline phase might liberate trapped volatiles which could then drive weak cometary outgassing (Bar-Nun & Laufer 2003). Of these volatiles, carbon monoxide (CO) is the most important, abundance-wise, in many comets (Biver et al. 2002a). Given its high abundance, it is reasonable to ask whether observational evidence for CO can be discerned at distances beyond the water sublimation zone. In fact, there exists a long record of observations of comets showing dust comae and tails when far beyond 5 AU, accompanied by speculation as to the role of CO and other supervolatiles in driving the mass loss. Currently (2007 August), nine cometary Centaurs (all by definition having perihelia outside the orbit of Jupiter) are known. The role of CO in driving this activity, however, is not uniquely established other than by direct spectroscopic detections reported in one or two cases (Senay & Jewitt 1994; Womack & Stern 1999).

The observability of CO at radio wavelengths depends on its volatility, the latter guaranteeing that CO ice will sublimate throughout the planetary region of the solar system when exposed to sunlight, and on the distribution of the populations of its rotational energy levels. For the pure collisional equilibrium case, the latter is given by the Boltzmann distribution,

$$f_J = \frac{(2J+1)e^{-\chi_J/kT}}{\Sigma_i (2i+1)e^{-\chi_i/kT}}. \quad (1)$$

This gives f_J, the fractional population of the Jth rotational level, as a function of χ_J, the energy of the level, and T, the kinetic temperature of the CO coma. The sum in the denominator of Equation (1) (the "partition function") is taken over all rotational levels. For plausible values of T the low J levels are highly populated over a wide range of heliocentric distances, a fact first highlighted by Crovisier et al. (1992). Physically,

* Observations conducted at the James Clerk Maxwell Telescope, which is operated by The Joint Astronomy Centre on behalf of the Particle Physics and Astronomy Research Council of the United Kingdom, The Netherlands Organisation for Scientific Research, and the National Research Council of Canada.

[1] Present address: Natural Sciences Department, Castleton State College, Castleton, VT 05735, USA.

[2] Present address: CNRS FRE 2591, Saclay, Bat 709, Orme des merisiers, 91191 Gif-sur-Yvette, France.

the relation between the rotational temperature in Equation (1) and the kinetic temperature is uncertain, depending on whether thermal equilibrium is attained in the coma.

The kinetic temperature is expected to be far below the local blackbody temperature as a result of two effects. First, as discussed below, the active surface will be cooled by sublimation relative to the blackbody temperature. Second, gas expanding from the source will be further cooled by adiabatic expansion. Practically, uncertainties about the temperature arise because the gas could be heated by entrained dust, or by percolation through a surface mantle on the nucleus that is itself heated by the Sun. The appropriate rotational temperatures are still less easy to determine from first principles, since collisional excitation, infrared pumping by solar radiation, and spontaneous decay are all important, and the relative contributions vary with distance from the nucleus and from the Sun. However, very low rotational temperatures have been inferred from line strength ratios in comets 29P/Schwassmann–Wachmann 1 (hereafter 29P/SW1) near $R = 6$ AU ($T \leqslant 10$ K; Crovisier et al. 1995) and in C/Hale–Bopp near $R = 10$ AU ($T = 8$ K; Gunnarsson et al. 2003). Here, we study the $J = 2$–1 transition of CO and employ $T = 10$ K throughout this paper, for which $f_2 = 0.24$. At $T = 50$ K, Equation (1) gives $f_2 = 0.19$, showing that a large uncertainty (factor of 5) in the temperature introduces a comparatively modest uncertainty in the derived production rates (factor of 1.3), which is unimportant for the purposes of our study.

In this paper we present observations taken in search of the CO $J = 2$–1 rotational line in a set of 12 Centaurs and Kuiper belt objects (KBOs). We combine our data with observations of ten other distant objects reported independently by Bockelee-Morvan et al. (2001) to derive constraints on the allowable CO mass loss rates. Then, we consider the implications of the CO line observations for the interior abundances of CO in these cometary precursor populations.

2. OBSERVATIONS

Observations were taken between January and August, 2002, at the James Clerk Maxwell Telescope (JCMT) on Mauna Kea, Hawaii. The JCMT is a 15 m diameter telescope equipped to observe primarily in the $0.45 \leqslant \lambda \leqslant 2$ mm wavelength range. We used the A3 receiver, whose 211–276 GHz spectral bandpass includes the 230.538 GHz (1.3 mm) $J = 2$–1 rotational transition of the CO molecule, and the digital autocorrelation spectrometer (DAS) backend. The channel spacing was 78 kHz, corresponding to a velocity resolution $\sim$0.10 km s^{-1} per channel. This stable instrument delivers a double sideband receiver temperature near 70 K at the CO frequency. Based on measurements of CO $J = 2$–1 in other sources in the upper and lower sidebands, we take the sideband gain ratio to be 1.0 ± 0.1. The half-power beam-width of A3 at 230 GHz is 20.8 arcsec, while the aperture efficiency is $\eta_A = 0.59$. Absolute calibration of the pointing was obtained using measurements of position standards (a variety of quasars and galactic sources) that were repeated on a 1–1.5 h basis. The instantaneous accuracy of the pointing determined from these measurements was near ± 1.5 arcsec, which is small compared to the beam width and therefore photometrically unimportant. Tracking on the solar system targets was achieved using software to interpolate linearly between start and end positions obtained from the JPL Ephemeris web site "Horizons." Given that we made no detections in the present program, it is important to note that the non-sidereal tracking capabilities of the JCMT were repeatedly verified through line detections of various planets and comets and continuum observations of asteroids and Kuiper belt objects (20000) Varuna and (134340) Pluto. Photometric calibration was obtained using the chopper wheel method, in which the spectrograph is exposed periodically to a metal disk of known temperature, and was checked via observations of standard galactic sources (mostly evolved stars with well-calibrated spectra).

Most of the data were taken as a back-up program, at times when the normal high frequency targets of the JCMT were unobservable because of atmospheric conditions. The current spectra were obtained with typical atmospheric vertical optical depths at 230 GHz in the range $0.14 \leqslant \tau_{230} \leqslant 0.26$, corresponding to water column abundances in the 2.8–5.2 mm range. Sky cancellation for all but two objects was obtained by position-switching the entrance aperture of the spectrometer by a distance 60–120 arcsec. The two targets (20000) Varuna and 1996 GQ21 were observed using frequency switching, in which the reference frequency of the receiver is shifted by 8.2 MHz without changing the position of the spectrometer beam on the sky.

Careful correction for the geocentric changing velocity is needed because of the very narrow Doppler line widths expected on the basis of the low gas temperatures. The spectra of each object, typically consisting of ten integrations of 60 s each, were averaged after shifting to correct for minute-to-minute changes in the geocentric velocity. The resulting composite spectra were then "baselined" by subtracting linear fits to regions ± 20 km s^{-1} from the nominal location of the CO $J = 2$–1 line. We experimented with baselines determined from other spectral windows and found that the choice of the fitted region and the method of the fit were not critical to the successful removal of the (very slight) deviations from linearity in the position-switched data. Larger curvature was present in the frequency-switched data as a result of the broad wings of telluric CO. For these, linear fits were inadequate and we employed second-order polynomials to fit the baseline. The combined spectra of each object are shown in Figure 1.

Observations of CO in 29P/SW1 at heliocentric distance $R \sim 6$ AU and in C/Hale–Bopp from $R \sim 6$ AU to 10 AU show that the CO line is structured with a core FWHM $\sim$100 m s^{-1} and a skirt extending to $\sim$500 m s^{-1} (e.g. Senay & Jewitt 1994; Crovisier et al. 1995; Festou et al. 2001; Gunnarson et al. 2003). The line is also blue-shifted with respect to the geocentric velocity by $\sim$400–500 m s^{-1} as a result of the ejection of the gas predominantly from the (Sun- and Earth-facing) day-side of the nucleus. We expect that CO lines from the Centaurs and KBOs should be similarly narrow and blue-shifted. Accordingly, in setting limits to the presence of the CO line we first measured the root-mean-square value of the temperature fluctuations within ± 20 km s^{-1} of the expected line velocity, and then scaled this to a 1 km s^{-1} wide box at the expected line location.

Table 1 lists the observed objects in order of increasing perihelion distance, giving the orbital semimajor axis, a, eccentricity, e, and inclination, i, for each object as well as a classification based on these parameters. The cometary designation given to Centaur 2002 T4 reflects the detection of a dust coma around this object in optical data (Bauer et al. 2003). The derived 3σ limits to the line area are listed in Table 2, together with parameters relevant to the spectra.

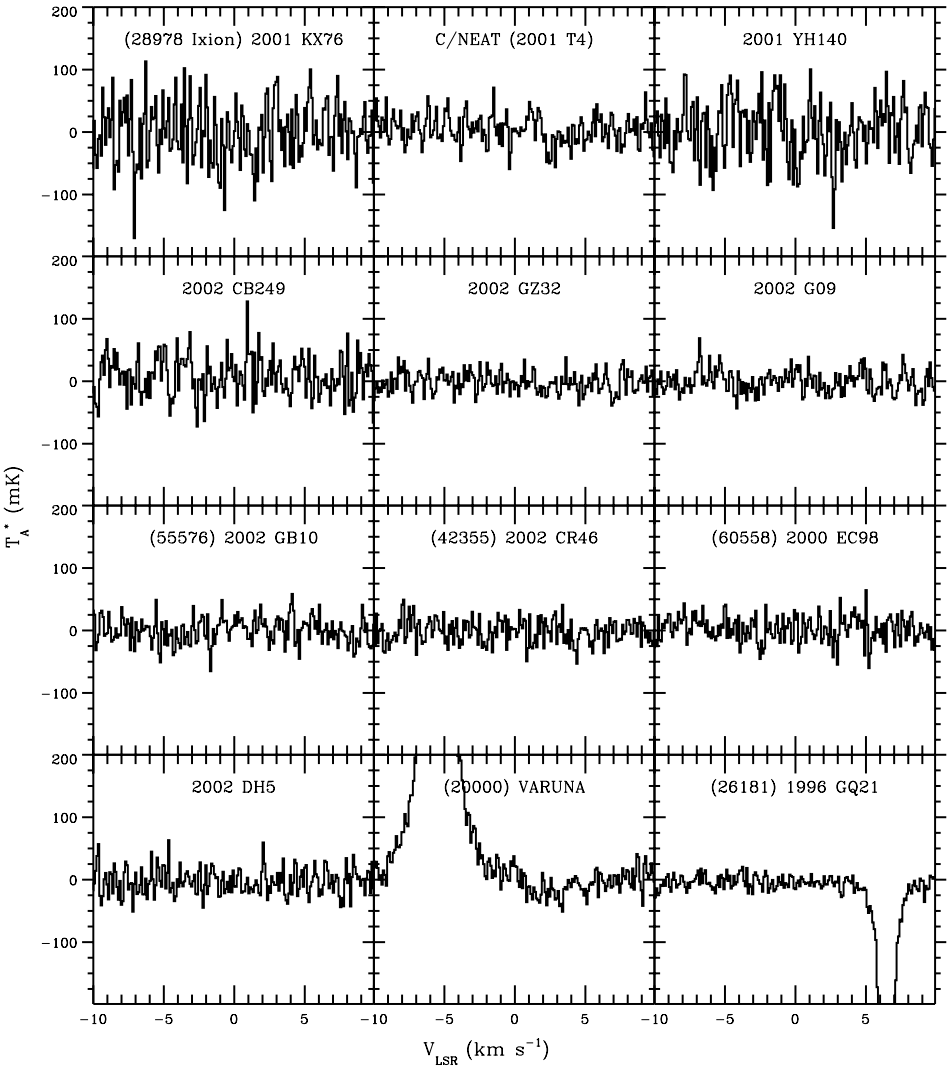

Figure 1. Spectra used to derive limits to the CO $J = 2$–1 emission line in the target sources. The spectra are shifted so that the expected velocity of each line falls at 0 km s^{-1} and are plotted on a common scale for ease of comparison. Large-scale features in the panels for (20000) Varuna and (26181) 1996 GQ21 are caused by telluric CO which is imperfectly removed in these frequency-switched data.

Table 1
Orbital Parameters of Observed Objects

Object	a[a]	e[b]	i[c]	q[d]	Type[e]
60558 (2000 EC98)	10.719	0.456	4.3	5.831	Centaur
C/NEAT (2001 T4)	13.903	0.384	15.4	8.564	Centaur Comet
2002 CB249	28.423	0.511	14.0	13.899	Scattered KBO
2002 DH5	22.195	0.370	22.4	13.983	Scattered KBO
2002 GO9	19.390	0.276	12.8	14.038	Centaur
55576 (2002 GB10)	25.144	0.396	13.3	15.187	Scattered KBO
42355 (2002 CR46)	38.299	0.542	2.4	17.541	Scattered KBO
2002 GZ32	23.134	0.218	15.0	18.091	Centaur
28978 Ixion (2001 KX76)	39.352	0.248	19.7	29.593	Plutino
2001 YH140	42.678	0.147	11.0	36.404	Classical KBO
(26181) 1996 GQ21	92.183	0.585	13.4	38.256	Scattered KBO
(20000) Varuna	43.058	0.057	17.1	40.604	Classical KBO

Notes.
[a] Orbital semimajor axis in AU.
[b] Orbital eccentricity.
[c] Orbital inclination in degrees.
[d] Perihelion distance in AU.
[e] Object type.

Table 2
Journal of Observations

Object	UT 2002[a]	t[b]	R[c]	Δ[d]	α[e]	τ_{230}[f]	$\int T_A^* dv$[g]
(60558) 2000 EC98	May 27, 29, 31	21040	14.826	14.527	3.8	0.15–0.20	0.017
C/NEAT (2001 T4)	Aug. 22, 24	13200	8.571	8.144	6.3	0.15–0.18	0.021
2002 CB249	Apr. 23	8580	13.901	13.269	3.3	0.16–0.22	0.028
2002 DH5	May 30, 31	16800	14.523	14.614	4.0	0.14–0.18	0.023
2002 GO9	May 22, 23	20100	14.038	13.201	2.4	0.15–0.20	0.016
(55576) 2002 GB10	May 24, 25	25200	15.201	14.650	3.2	0.17–0.25	0.020
(42355) 2002 CR46	May 27, 29, 30	16210	18.051	18.586	2.7	0.15–0.20	0.019
2002 GZ32	May 21, 22, 23	27160	21.123	20.641	2.4	0.13–0.20	0.016
(28978) Ixion	Mar. 13	4200	43.150	42.870	1.3	0.17–0.23	0.045
2001 YH140	Apr. 23	4170	36.405	6.690	1.5	0.18–0.20	0.041
(26181) 1996 GQ21	Jan. 10, 11, 12, 13	54000	39.408	39.620	1.4	0.13–0.18	0.010
(20000) Varuna	Jan. 9, 10	20400	43.208	42.810	1.2	0.13–0.18	0.015

Notes.
[a] UT Dates of observation.
[b] Total integration time in seconds.
[c] Average heliocentric distance in AU.
[d] Average geocentric distance in AU.
[e] Phase angle in degrees.
[f] Atmospheric optical depth at 230 GHz.
[g] 3σ upper limit to the line area in K km s^{-1} in a 1 km s^{-1} band.

3. RESULTS

The rate of emission of photons in the $J = 2$–1 line is given by $f_2 A_{21} N$ (s^{-1}), where f_2 is the fraction of the CO molecules in the $J = 2$ rotational level, $A_{21} = 7.2 \times 10^{-7}$ s^{-1} is the Einstein A coefficient for the transition to $J = 1$, and N is the total number of CO molecules within the spectrometer beam. We write $N = Q_{\rm CO}\tau_r$, where $Q_{\rm CO}$ (s^{-1}) is the sought-after production rate of CO molecules and τ_r (s) is the time of residence of each CO molecule within the beam. An absolute upper limit to τ_r is set by the lifetime of the CO molecule against photodestruction, $\tau_{\rm ph}$. The latter is given by $\tau_{\rm ph} = 3.6 \times 10^6 R^2$, where R is the heliocentric distance measured in AU (Huebner et al. 1992). Even for the closest of our targets (2001 T4 at $R = 8.57$ AU) we find $\tau_{\rm ph} = 2.6 \times 10^8$ s (about 10 years) so that for all practical purposes we can ignore photodestruction. Instead, the residence time is set by the speed of outflow of the CO molecules as they stream away from their source. Therefore, to determine limits on the CO production rate we need to model the outflow of molecules across the projected spectrometer entrance aperture. For an isotropic source, the mean residence time within a circular aperture of radius $L = \theta\Delta$ km is (to within a factor of order unity) $\tau_r = \theta\Delta/v_o$, where Δ (m) is the geocentric distance, θ is the aperture radius expressed in radians, and v_o is the ejection speed. At the JCMT, the relation between the measured antenna temperature, T_A^* (K), and the flux density, S_ν (W m^{-2} Hz^{-1}), is given by $S_\nu = 15.6 \times 10^{-26}\, T_A^*/\eta_A$ (JCMT Observing Manual, part 5: Observing spectral lines, published online at http://docs.jach.hawaii.edu/JCMT/HET/GUIDE/het_guide/). Substituting and rearranging, we obtain

$$Q_{\rm CO} = 1.48 \times 10^{15} \left[\frac{v_o(R)\Delta \int T_A^* dv}{f_2 A_{21} \eta_A \theta} \right] \qquad (2)$$

where Δ is expressed in AU, the integral gives the line area, and the other symbols are as previously defined. The f_2 level population was computed from Equation (1).

What should we use for $v_o(R)$? On an inert (refractory) body heated by the Sun, the temperature varies with heliocentric distance as $T \propto R^{-1/2}$ and the corresponding thermal velocity of molecules should then scale as $v_o(R) \propto T^{1/2} \propto R^{-1/4}$. The mean temperature of the surface at any given R will be a function of the shape, rotation vector, and thermal diffusivity of the material of the body. If the surface is volatile, the temperature will be depressed owing to energy used in driving the sublimation. As an extreme example, we have solved the energy balance equation as a function of R for a perfectly absorbing patch of CO ice located at the sub-solar point of a non-rotating body and illuminated normally by the Sun. Sublimation power completely dominates radiation power, and the resulting temperature is essentially isothermal near $T \sim 26$ K throughout the planetary region of the solar system. The corresponding thermal speed of the CO molecules is then $v_o(R) \sim 150$ m s^{-1}, independent of R. This relation is plotted in Figure 2 (curve (a)). Neglecting sublimation, we next consider the maximum (sub-solar) temperature on a non-rotating body, to find $T = 393\, R^{-1/2}$ and $v_o(R) = 590\, R^{-1/4}$ (m s^{-1}): this relation is shown in Figure 2 (curve (b)). Measurements of the outflow speed in comets 29P/SW1 (Senay & Jewitt 1994) and C/Hale–Bopp (Biver et al. 2002b) show that the measured gas speed, $v_o(R)$ (Figure 2), is slightly higher than given by curve (b). The reasons for this are not entirely clear, but may be connected with heating of the gas as it flows through a refractory mantle, or heating by entrained dust grains. We resort to the empirical relation found from measurements of CO in C/Hale–Bopp over the distance range $4 \leqslant R \leqslant 14$ AU (Biver et al. 2002b; curve (c) in Figure 2), namely

$$v_o(R) = 853 R^{-1/4}. \qquad (3)$$

The speed given by Equation (3) is large compared to the gravitational escape speeds of the observed bodies (other than (28978) Ixion) and so we reject the possibility that CO at these objects might be trapped in quasi-bound atmospheres (as at (134340) Pluto). In (28978) Ixion, the possibility that CO might be gravitationally trapped means that the production rate derived in this paper is a strong upper limit to the actual rate.

The limiting $Q_{\rm CO}$ production rates for each object obtained from Equations (1) through (3) are summarized in Table 3. As noted above, the production rate was calculated assuming $T = 10$ K: rates computed assuming $T = 50$ K are larger by a factor of

Table 3
Production Rate Limits

Object	H_V [a]	$D_{0.1}$ [b]	Q_{CO} [c]	γ [d]	$\phi \times 10^{-3}$ [e]	$\tau_v \times 10^4$ [f]
(60558) 2000 EC98	9.5	55	3.1×10^{28}	58	7	1.2
C/NEAT (2001 T4)	$\geqslant$11.7	$\leqslant$20	2.4×10^{28}	18	–	–
2002 CB249	9.8	48	4.8×10^{28}	95	13	1.3
2002 DH5	10.2	40	4.1×10^{28}	88	18	1.3
2002 GO9	9.3	60	2.8×10^{28}	55	5	1.0
(55576) 2002 GB10	7.8	120	3.7×10^{28}	86	2	1.5
(42355) 2002 CR46	7.2	157	4.0×10^{28}	134	1	2.5
2002 GZ32	6.9	181	3.8×10^{28}	175	17	4.0
(28978) Ixion	3.2	993	18.9×10^{28}	3600	1	75
2001 YH140	5.5	344	15.0×10^{28}	2040	6	40
(26181) 1996 GQ21	5.15	410	3.9×10^{28}	624	1	26
(20000) Varuna	3.47	880	6.3×10^{28}	1200	0.5	43

Notes.
[a] Absolute V-band magnitude. Data from the Minor Planet Electronic Circulars except for 2001 T4, which are based on unpublished Mauna Kea photometry.
[b] Diameter (km) derived from H on the assumption that the V-band geometric albedo is 0.1.
[c] Limit to the CO (s^{-1}) production rate derived from the spectra in Figure 1 assuming $T = 10$ K (see Table 2).
[d] The area (in km^2) of an exposed, black CO slab that would be needed to sublimate at the limiting rate given in the previous column, computed from Equation (4).
[e] The maximum fraction of the surface area that could be covered by Sun-facing CO and not violate the spectral limits to outgassing, computed from Equation (6) and expressed in thousands. No value is given for 2001 T4 because we possess only a limit to the diameter.
[f] Lifetime of the CO vent to self-shadowing in units of 10^4 years, computed from Equation (7).

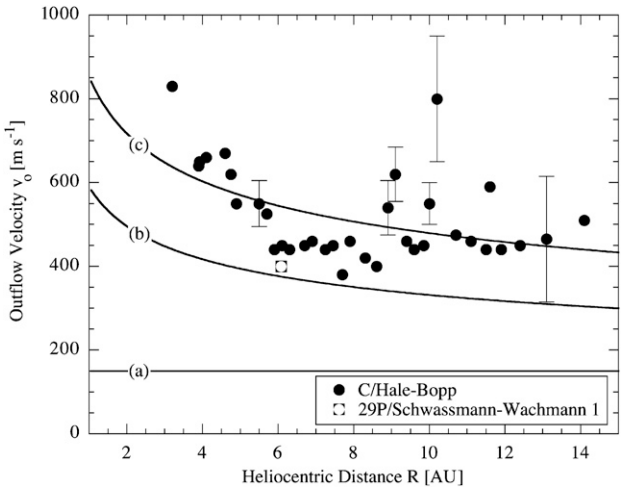

Figure 2. Carbon monoxide outgassing velocity as a function of heliocentric distance. The data for C/Hale–Bopp (circles) are from Biver et al. (2002b). Error bars are plotted where they substantially exceed the size of the symbols used to plot the data. The (empty square) point for 29P/Schwassmann–Wachmann 1, from Senay & Jewitt (1994), is representative of a large number of CO measurements of this object taken at nearly constant heliocentric distance. Three models are shown as lines: (a) the thermal velocity expected of CO molecules sublimating freely in thermal equilibrium with sunlight, (b) the velocity expected if the local temperature is that of an inert body, again in thermal equilibrium (see the text), and (c) the best-fit to the Hale–Bopp data, $v_o = 853\ R^{-1/4}$, proposed by Biver et al. (2002b).

about 1.3. The gas outflow velocity may be further uncertain by a factor of $\sim$2; it is a simple matter to scale the production rates for any other value of the velocity using Equation (2). Figure 3 shows the Q_{CO} limits as a function of the heliocentric distance, with data from Table 3 shown alongside data for Centaurs and KBOs from Bockelee-Morvan et al. (2001). Additionally, values of Q_{CO} measured in C/Hale–Bopp are overplotted on the figure. Numbers on the right hand axis show the CO mass production rates computed from $dm_{CO}/dt = \mu m_H Q_{CO}$, with molecular weight $\mu = 28$ and hydrogen mass $m_H = 1.67 \times 10^{-27}$ kg. The blue lines in Figure 3 are trajectories for the Q_{CO} limits corresponding to line areas $\int T_A dv = 0.01$, 0.05, and 0.25 K km s^{-1}, computed for observations taken at opposition (i.e., $\Delta = R - 1$).

4. DISCUSSION

Outgassing of CO has been previously reported in two Centaurs, namely the continuously active cometary Centaur 29P/SW1 and (2060) Chiron. The emission in 29P/SW1 is strong, with the $J = 2$–1 line having $\int T_A dv = 0.08 \pm 0.01$ K km s^{-1} at $R \sim 6$ AU (Senay & Jewitt 1994; Croviser et al. 1995; Festou et al. 2001). The mass loss rate in CO from this object is steady at 1–2 t s^{-1}. In (2060) Chiron at $R = 8.5$ AU, Womack & Stern (1999) reported a CO $J = 1$–0 line area 0.0135 ± 0.0027 K km s^{-1}, corresponding to derived production rate $Q_{CO} = 1.5 \pm 0.8 \times 10^{28}$ s^{-1}. We reanalyzed the data from Figure 1 of Womack & Stern (1999) to determine the standard deviation in their spectrum as $1\sigma = 0.010$ K per 100 kHz (0.26 km s^{-1}) resolution element. The two channels reported by Womack & Stern as CO stand 0.028 K and 0.019 K above zero, corresponding to 2.8σ and 1.9σ, respectively. Their combined significance is 3.4σ, assuming that all the signal is, and should be, in these two channels alone. This is less than the 5σ result claimed by the authors, but remains a formal detection of the line provided only the signal from those two channels is considered. Unfortunately, unlike the observations of CO in 29P/SW1, the detection in (2060) Chiron has not been confirmed in deeper observations by others (Rauer et al. 1997; Bockelee-Morvan et al. 2001). Separately, optical emission from the CN radical

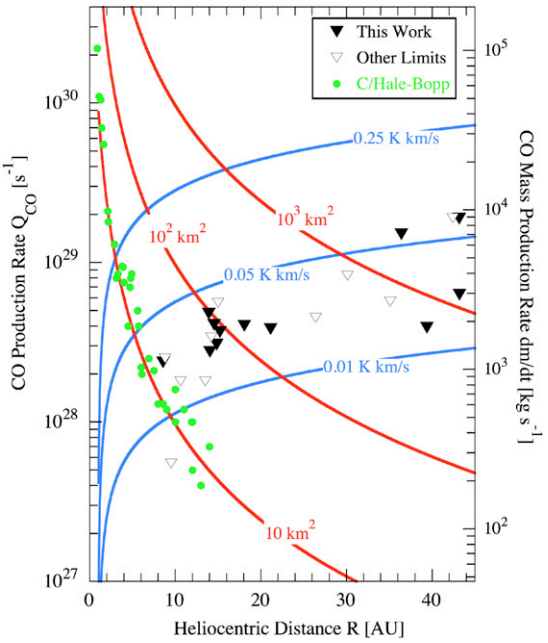

Figure 3. Carbon monoxide production rates as a function of heliocentric distance. Downward pointing triangles indicate upper limits: filled triangles from the present work (see Table 3) and empty triangles from Bockelee-Morvan et al. (2001). Green circles indicate post-perihelion CO production rates from comet C/Hale–Bopp, as reported by Biver et al. (2002b). Blue lines show models for the production rates corresponding to CO $J = 2$–1 line areas 0.01, 0.05, and 0.25 K km s^{-1}. Red lines show the equilibrium sublimation rates from exposed areas of CO of 10, 100, and 1000 km^2.

has been reported in Chiron (Bus et al. 1991) but this observation is also unconfirmed.

A simple summary of the observations, then, is that CO is undetected in the 22 Centaurs and Kuiper belt objects observed by us and by Bockelee-Morvan et al. (2001), is strongly detected on many occasions in one Centaur (29P/SW1), and has been marginally detected, but only once, in another (Chiron).

4.1. Bulk CO Ice

Carbon monoxide ice is exposed on the surface of the large Kuiper belt object (134340) Pluto (Owen et al. 1993) and on Neptune's satellite Triton (Cruikshank et al. 1993). The survival and distribution of surface volatiles on these large bodies is aided by their gravity and the thin, sublimation-driven atmospheres from which surface frosts may be deposited. Bound atmospheres are unlikely to be found on the smaller KBOs and Centaurs. Still, the likely origin of the Centaurs in the Kuiper belt means that we cannot discount the possibility that transient exposures of solid CO ice exist on newly arrived Centaurs. We first address the empirical upper limits that can be placed on the maximum area of exposed CO ice on these bodies. In a later section, we address the (more likely) possibility that CO is physically trapped within an amorphous water ice host, not present as a free ice.

As noted earlier, CO ice is highly volatile and most of the energy absorbed from the Sun is used in breaking bonds between CO molecules in sublimation. The energy balance equation in this case is simply

$$\frac{F_\odot \gamma}{R^2} = \mu m_H L_{\rm CO} Q_{\rm CO} \quad (4)$$

in which $L_{\rm CO}$ (J kg^{-1}) is the latent heat of sublimation of CO, $F_\odot = 1360$ W m^{-2} is the solar constant, and γ is the effective sublimating area. We take $L_{\rm CO} = 3 \times 10^5$ J kg^{-1} (Brown & Ziegler 1979) and $\mu = 28$ to estimate γ for each object in our sample (Table 3). Equation (4) was used to plot $Q_{\rm CO}$ as a function of R for areas $\gamma = 10, 10^2$, and 10^3 km^2 in Figure 3. The figure shows that carbon monoxide sublimation from an area $\gamma \sim 10$–20 km^2 provides a rather good fit to the C/Hale–Bopp data over three orders of magnitude in production rate (cf. Jewitt et al. 1996; Biver et al. 2002b). Given the $D \sim 40$ km diameter of the nucleus of this comet (Fernandez 2002), the fraction of the nucleus surface area that must be covered by CO in order to produce $Q_{\rm CO}$ is $\phi = \gamma/\pi D^2 \sim 0.2$–0.4%. In 29P/SW1, the corresponding numbers are $\gamma \sim 20$ km^2, $D \sim 20$–30 km, and $\phi \sim 0.7$–1.5% (Senay & Jewitt 1994). If we take the Womack & Stern (1999) detection as real, we obtain $\gamma \sim 11$ km^2 and, with $D = 200$ km, obtain $\phi \sim 10^{-4}$ for (2060) Chiron.

The sizes of the newly observed objects are not well determined at the time of writing. We list the absolute magnitudes, H_V, in Table 3 and derive diameters on the assumption that the geometric, V-band albedo is 0.1, using the inverse square law expressed as

$$\frac{D}{100\ {\rm km}} = 10^{0.2(8.2-H_V)}. \quad (5)$$

From Equation (4), the maximum fraction of the surface of each object which could then consist of exposed, freely sublimating CO ice is given by

$$\phi = \frac{\mu m_H L_{\rm CO} Q_{\rm CO} R^2}{F_\odot \pi D^2}, \quad (6)$$

and this fraction is also listed in Table 3. These expressions are clearly approximate in nature, because Equation (4) neglects thermal conduction and assumes that the exposed CO patch is normal to the Sun. Still, the derived effective areas in Table 3 are interesting in that they correspond to very small fractions of the total areas of the bodies: the surfaces of Centaurs and KBOs are strongly depleted in supervolatile ices.

This result is easy to understand. Exposed CO should sublimate rapidly, causing the sublimation surface to quickly recede beneath adjacent, non-sublimating areas to form a crater or pit. The rate of sublimation is readily calculated from Equation (4). Self-shadowing of the floor of the crater will lead to a maximum depth on the order of the diameter of the crater and, soon thereafter, to the deactivation of the vent. The limiting vent diameters estimated from $d_v \sim \gamma^{1/2}$ (Table 3) are typically from a few to 10 km on the Centaurs, and from 30 to 40 km on the more distant objects. The vent lifetimes to self-shadowing are given, to order of magnitude, by

$$\tau_v \sim \frac{\rho R^2 \gamma^{1/2} L_{\rm CO}}{F_\odot}, \quad (7)$$

where ρ (kg m^{-3}) is the bulk density (we assume $\rho = 1000$ kg m^{-3}). This quantity is also listed in Table 3. These lifetimes are clearly based on very crude assumptions about the structure of active CO vents. For instance, if sublimation can proceed through the walls of a pit (as suggested by high resolution observations of cometary nuclei; Basilevsky & Keller 2006), then τ_v may exceed the value given by Equation (7) by a considerable margin even if the floor is permanently shadowed. Still, the long-term survival of CO ice exposed to the heat of the Sun on the surface of a Centaur is very unlikely.

The derived lifetimes are all very short compared to the $\sim 4.5 \times 10^9$ yr age of the Solar system and short compared

to the median dynamical lifetime of bodies escaped from the Kuiper belt, namely $\tau_{\rm dyn} \sim 10^7$ year (Tiscarano & Malhotra 2003; Horner et al. 2004). This means that CO could persist on the surfaces of these bodies only if it has been emplaced there in recent times. Excavation by impact is an unlikely mechanism, given that the Centaur regime is collisionally benign (Durda & Stern 2000). More likely is the possibility that CO lies buried in Kuiper belt objects, where it is shielded from the heat of the Sun by overlying porous, refractory matter. The thermal skin depth corresponding to the $P \sim 250$ yr orbital period of a representative KBO with semimajor axis 40 AU is of order $d_{\rm th} \sim (P\kappa)^{1/2}$, where κ (m^2 s^{-1}) is the thermal diffusivity. For a porous material with $\kappa \sim 10^{-7}$ m^2 s^{-1}, this depth is $d_{\rm th} \sim 30$ m. Average temperatures at depth d would be attenuated from that at the surface by a factor $e^{-\frac{d}{d_{\rm th}}}$, allowing CO and other supervolatiles to survive as ice at depths $d \geqslant d_{\rm th}$. In the larger objects, especially, outward migration of CO due to temperature gradients created by the decay of radioactive nuclei and inward diffusion from the surface region due to solar heating would produce a layer of concentrated CO (and other supervolatile) ice at depths $d \sim 1$ km (Yabushita 1995; Choi et al. 2002; Merk & Prialnik 2006).

The short vent lifetimes indicated by Equation (7) (see Table 3) argue that outgassing from individual exposed patches of the surface should be short-lived. If we take the typical vent lifetime for Centaurs from Table 3 to be $\tau_v \sim 10^4$ yr and the dynamical time to be $\tau_{\rm dyn} \sim 10^7$ yr, then one would expect the fraction of Centaurs to be outgassing at any given time to be only $\tau_v/\tau_{\rm dyn} \sim 10^{-3}$, and no examples would be expected in the current Centaur sample of ~70 objects (since $70 \times 10^{-3} \ll 1$). In fact, the nine known cometary Centaurs correspond to about 15% of the observed population. One reconciliation of the large fraction of active Centaurs with the small expected vent lifetimes is presumably that while individual vents are short-lived, different vents may be activated at different times and places on each Centaur. This is consistent with evidence from the nuclei of short-period comets: the nuclei typically outgas from several discrete locations distributed over the surface and activated at different times by rotational and seasonal variations in the insolation. On longer timescales, irregularities in the shapes of the Centaurs and inhomogeneities of the internal structure will interact with the slowly propagating thermal conduction wave to activate buried volatiles at different times and locations. A second but not well-quantified contributor to the high fraction of active Centaurs is that there is an observational bias in favor of finding outgassing Centaurs because these are brighter and, therefore, more readily detected in optical surveys than their point-like, inactive counterparts.

Despite their greater distances and lower temperatures, the CO vent lifetimes on KBOs (cf. Table 3) are still short compared to the likely timescale for the collisional activation of vents large enough to generate measurable CO emission. For example, the $\gamma \sim 10^3$ km^2 limiting areas derived for KBOs from Equation (4) correspond to sublimation from exposed patches of CO that are $\gamma^{1/2} \sim 30$ km in extent. If we suppose that these are craters, then the implied projectile dimensions are near 3–5 km. The most optimistic estimates for the timescale for the collision of projectiles of this size into the observed KBOs are $\tau_C \sim 10^9$ yr (cf. Durda & Stern 2000), which is sufficiently long that we should not expect to find any currently active examples, consistent with the null detections reported here and in Bockelee-Morvan et al. (2001).

4.2. Physically Trapped CO

Lastly, we consider the possibility that the loss of CO from bodies in the outer solar system is controlled by the physical binding of CO molecules within a structure defined by other ices, principally water ice. This phenomenon is seen in laboratory experiments in which solids that are formed by low ($\leqslant$80 K) temperature condensation release trapped volatiles, including CO, at discrete temperatures corresponding to changes in the crystalline structure of water ice (e.g., Bar-Nun & Laufer 2003). For example, there is an effusion of CO at temperatures 135–155 K, corresponding to rearrangement of the structure from amorphous ice to the crystalline form. These temperatures approximate the sub-solar temperature on a black, non-rotating body at heliocentric distances $6 \leqslant R \leqslant 8$ AU. All but two of the objects in Table 1 have perihelia beyond this critical range. Therefore, a self-consistent alternative interpretation of the data is that CO outgassing is not detected on most Centaurs and KBOs because the objects are too distant and too cold to trigger the amorphous-to-crystalline phase transition. Detection of CO in 29P/SW1 is qualitatively compatible with this scenario, since its perihelion distance, $q = 5.7$ AU, lies inside the critical distance range. (2060) Chiron, $q = 8.5$ AU, falls at the outer boundary of the critical distance range for initiation of the phase transition. C/NEAT (2001 T4) has a dust coma (but no CO was detected, see Figure 1) and has a similar $q = 8.6$ AU (Table 3). The rapid on-set of CO production from C/Hale–Bopp near $R \sim 6$ AU (Jewitt et al. 1996; Biver et al. 2002b) is likewise consistent with the release of CO at a rate controlled by the thermodynamics of amorphous water ice (Prialnik 1997a, 1997b). Interestingly, near-infrared spectral observations of C/Hale–Bopp indeed suggest the presence of amorphous water ice in the grains of its coma (Davies et al. 1997). None of these examples rises to the level of a formal proof that the CO is released from an amorphous water ice matrix, but the data appear consistent with the possibility.

Laboratory experiments with slowly heated amorphous ice samples further show that gas is released at temperatures below the major phase transition at 135–155 K, apparently due to annealing within the sample. The ratio of the number of molecules released during the annealing phase to the number released by the runaway amorphous-to-crystalline phase transition is of order 1/20 (Bar-Nun 2004, personal communication). Could such low-level outgassing be detected in the Centaurs? To take the best example, 29P/SW1 is known to maintain a steady CO production rate near $dM/dt = 1000$–2000 kg s^{-1}. Suppose that both the perihelion distance and this rate of mass loss have been stable for $\tau_p \sim 10^3$ yr, a small fraction of the $\tau_{\rm dyn} \sim 10^7$ yr dynamical transport time from the Kuiper belt (Tiscarena & Malhotra 2003; Horner et al. 2004). Then, if annealing occurred over the full dynamical transport time the average rate of production of CO due to annealing prior to the phase transition would be $dm/dt \sim \left[\tau_p/(20\tau_{\rm dyn})\right] dM/dt$, or about 0.01–0.02 kg s^{-1}. Outgassing at such a low rate would be completely undetectable by current spectroscopic means, consistent with the non-detection of CO from Centaurs other than 29P/SW1 and, perhaps, (2060) Chiron.

The main unknown of the amorphous water ice model for trapping of volatiles is whether or not the ice in comets, Centaurs, and KBOs is really amorphous to begin with. Indeed, published spectra of objects in the Kuiper belt—namely Charon (Buie & Grundy 2000), (50000) Quaoar (Jewitt & Luu 2004), and 2003 EL61 (Trujillo et al. 2007)—show crystalline, not

amorphous water ice, at least at the surface. If the ice is not amorphous to begin with, then clearly the physical trapping models for CO would be irrelevant. However, we cannot yet conclude that this is so. The caveat is that near infrared spectroscopy probes only a millimeter-thick surface skin; the nature of what lies beneath remains unknown.

5. SUMMARY

In this paper we present sensitive measurements of the radio spectra of 12 outer solar system objects taken in search of emission from the CO $J = 2$–1 rotational transition at 230 GHz. The only distant bodies in which CO outgassing has been previously reported are the Centaurs 29P/Schwassmann–Wachmann 1, where the outgassing is strong, variable ($2–4 \times 10^{28}$ s^{-1}, corresponding to about 1–2 t s^{-1}), and continuous, and (2060) Chiron, where the emission is weak (a $\sim 3\sigma$ detection of $\sim 1.5 \times 10^{28}$ s^{-1}, about 0.7 t s^{-1}), and the observation has not been independently confirmed. From our observations we find the following.

(1) No emission lines were detected at 3σ limiting sensitivities near 20 mK km s^{-1} in objects with heliocentric distances in the 8–43 AU range. The limiting CO mass loss rates derived from a simple model lie in the range $\sim 3 \times 10^{28}$ s^{-1} to $\sim 2 \times 10^{29}$ s^{-1}, corresponding to ~ 1 to 12 t s^{-1}.

(2) Two models for the production of CO are considered and compared with the data. If CO is assumed to be exposed as surface ice, then the non-detections limit the effective sublimating areas to $\sim$10–100 km^2 on the Centaurs, and $\sim 10^3$ km^2 on the more distant KBOs. Assuming sublimation in thermal equilibrium with sunlight, the fraction of the surface area occupied by CO ice is 0.1–1%, or less, meaning that the surfaces of the Centaurs and KBOs must be strongly depleted in supervolatile ices. Strong depletion is easily understood as a result of the extreme volatility of CO, which leads to rapid loss of exposed CO ice through sublimation. Pure CO ice could be stable, however, beneath a refractory surface mantle on these objects.

(3) In a more likely scenario, CO is instead held by physical trapping in an amorphous water ice host instead of being exposed as free ice at the surface. In this case, the outgassing of CO and other volatiles is controlled largely by the thermodynamics of the water ice, specifically of the transition from the amorphous to the crystalline phase. Then, the CO non-detections can be naturally understood as a consequence of the large perihelia and resulting low surface temperatures of the observed objects.

We thank Wei Hao Wang and Sebastien Lefranc for help with some of the observing. Maria Womack kindly discussed her (2060) Chiron observation with D.J. in detail and Akiva Bar-Nun, Jane Luu, Scott Sheppard, Rachel Stevenson, and the anonymous referee offered helpful comments on the manuscript. This work was supported by a grant to D.J. from the NASA Planetary Astronomy Program.

REFERENCES

Bar-Nun, A., & Laufer, D. 2003, Icarus, 161, 157
Basilevsky, A. T., & Keller, H. U. 2006, Planet. Space Sci., 54, 808
Bauer, J. M., Fernández, Y. R., & Meech, K. J. 2003, PASP, 115, 981
Biver, N., et al. 2002a, Earth Moon Planets, 90, 323
Biver, N., et al. 2002b, Earth Moon Planets, 90, 5
Bockelée-Morvan, D., Lellouch, E., Biver, N., Paubert, G., Bauer, J., Colom, P., & Lis, D. C. 2001, A&A, 377, 343
Brown, G., & Ziegler, W. 1979, Adv. Cryog. Eng., 25, 661–670
Buie, M. W., & Grundy, W. M. 2000, Icarus, 148, 324
Bus, S. J., A'Hearn, M. F., Schleicher, D. G., & Bowell, E. 1991, Science, 251, 774
Choi, Y., Cohen, M., Merk, R., & Prialnik, D. 2002, Icarus, 160, 300
Crovisier, J. 1992, in Workshop on the Activity of Distant Comets, ed. W. H. Huebner, D. Jewitt Keller, & J. Klinger (San Antonio, TX: Southwest Research Institute) 153–160
Crovisier, J., Biver, N., Bockelee-Morvan, D., Colom, P., Jorda, L., Lellouch, E., Paubert, G., & Despois, D. 1995, Icarus, 115, 213
Cruikshank, D. P., Roush, T. L., Owen, T. C., Geballe, T. R., de Bergh, C., Schmitt, B., Brown, R. H., & Bartholomew, M. J. 1993, Science, 261, 742
Davies, J. K., Roush, T. L., Cruikshank, D. P., Bartholomew, M. J., Geballe, T. R., Owen, T., & de Bergh, C. 1997, Icarus, 127, 238
Duncan, M., Quinn, T., & Tremaine, S. 1988, ApJ, 328, L69
Durda, D. D., & Stern, S. A. 2000, Icarus, 145, 220
Fernandez, J. A. 1980, MNRAS, 192, 481
Fernández, Y. R. 2002, Earth Moon Planets, 89, 3
Festou, M. C., Gunnarsson, M., Rickman, H., Winnberg, A., & Tancredi, G. 2001, Icarus, 150, 140
Gunnarsson, M., et al. 2003, A&A, 402, 383
Hartmann, W. K., Tholen, D. J., & Cruikshank, D. P. 1987, Icarus, 69, 33
Horner, J., Evans, N. W., & Bailey, M. E. 2004, MNRAS, 354, 798
Huebner, W. F., Keady, J. J., & Lyon, S. P. 1992, A&AS, 195, 1
Jewitt, D. 2005, in From Cradle to Grave: The Rise and Demise of the Comets. In COMETS II, ed. M. Festou, H. Weaver, & U. Keller (Tucson Az: Univ. Anizona Press) 659–676
Jewitt, D., Senay, M., & Matthews, H. 1996, Science, 271, 1110
Jewitt, D. C., & Luu, J. 2004, Crystalline water ice on the Kuiper belt object (50000) Quaoar, Nature, 432, 731
Kawakita, H., Watanabe, J., Ootsubo, T., Nakamura, R., Fuse, T., Takato, N., Sasaki, S., & Sasaki, T. 2004, ApJ, 601, L191
Merk, R., & Prialnik, D. 2006, Icarus, 183, 283
Owen, T. C., et al. 1993, Science, 261, 745
Prialnik, D. 1997a, ApJ, 478, L107
Prialnik, D. 1997b, Earth Moon Planets, 77, 223
Rauer, H., et al. 1997, Planet. Space Sci., 45, 799
Senay, M. C., & Jewitt, D. 1994, Nature, 371, 229
Tiscareno, M. S., & Malhotra, R. 2003, AJ, 126, 3122
Trujillo, C. A., Brown, M. E., Barkume, K. M., Schaller, E. L., & Rabinowitz, D. L. 2007, ApJ, 655, 1172
Whipple, F. L. 1950, ApJ, 111, 375
Womack, M., & Stern, S. A. 1999, Astron. Vestn., 33, 187
Yabushita, S. 1995, MNRAS, 273, 940